

## Supplementary Material for

### High Drag Reduction by Spontaneous Capture and Transportation of Bubble

Junyi Lin<sup>a</sup>, Xinming Wang<sup>a</sup>, Han Wang,<sup>a</sup> Zening Sun<sup>a</sup>, Defeng Yan<sup>c\*</sup>, and Jinlong Song<sup>a, b\*</sup>

<sup>a</sup> State Key Laboratory of High-performance Precision Manufacturing, Dalian University of Technology, Dalian Liaoning, 116024, China.

<sup>b</sup> Key Laboratory for Micro/Nano Technology and System of Liaoning Province, Dalian University of Technology, Dalian Liaoning, 116024, China.

<sup>c</sup> School of Mechanical Engineering, Dalian University of Technology, Dalian Liaoning, 116024, China.

\*Corresponding author: songjinlong@dlut.edu.cn; yandefeng@mail.dlut.edu.cn

## Content

### 1. Figure section

Figure S1. 3D schematic diagram of the underwater drag reduction test system.

Figure S2. Drag reduction rate of the SPSB at different water temperatures.

Figure S3. Surface roughness of the exterior area of the track for two types of surfaces.

Figure S4. Comparison of drag reduction rates between two different surfaces.

Figure S5. Boundary attribute setting of the SPSB numerical simulation model.

Figure S6. Grid division of the SPSB numerical simulation model.

Figure S7. Comparison of experimental and simulated results of the SPSB at a gas flux of  $0.5\text{L}\cdot\text{min}^{-1}$  and different water flow velocities.

Figure S8. Gas volume fraction cloud map of the SPSB.

Figure S9. Schematic diagram of anti-diatom attachment experimental device.

Figure S10. Image of pattern arrangement when the SPSB can achieve maximum anti fouling area.

### 2. Table section

Table S1: Average drag reduction rates of the SPSB at different gas fluxes and  $0.3\text{ m}\cdot\text{s}^{-1}$  water velocity.

Table S2: Average drag reduction rates of the SPSB at different gas fluxes and  $0.4\text{ m}\cdot\text{s}^{-1}$  water velocity.

Table S3: Average drag reduction rates of the SPSB at different gas fluxes and  $0.5\text{ m}\cdot\text{s}^{-1}$  water velocity.

Table S4: Average drag reduction rates of the SPSB at different gas fluxes and  $0.6\text{ m}\cdot\text{s}^{-1}$  water velocity.

Table S5: Average drag reduction rates of the hydrophobic Al surface at different gas fluxes and  $0.6\text{ m}\cdot\text{s}^{-1}$  water velocity.

Table S6: Average drag reduction rates of the untreated Al at different gas fluxes and  $0.6\text{ m}\cdot\text{s}^{-1}$  water velocity.

Table S7: The drag reduction methods used in existing research results and the achievable drag reduction rates.

### 3. Video section

Video S1. The transportation processes of the gas bubble on the SPSB.

Video S2. The gas layer states of the SPSB at different gas fluxes.

Video S3. The gas layer states of different surfaces.

Video S4. The gas layer states of different inclined surfaces.

Video S5 The experimental process of simulating barnacle larvae adhering to the untreated Al surface and SPSB.

## 1. Figure section

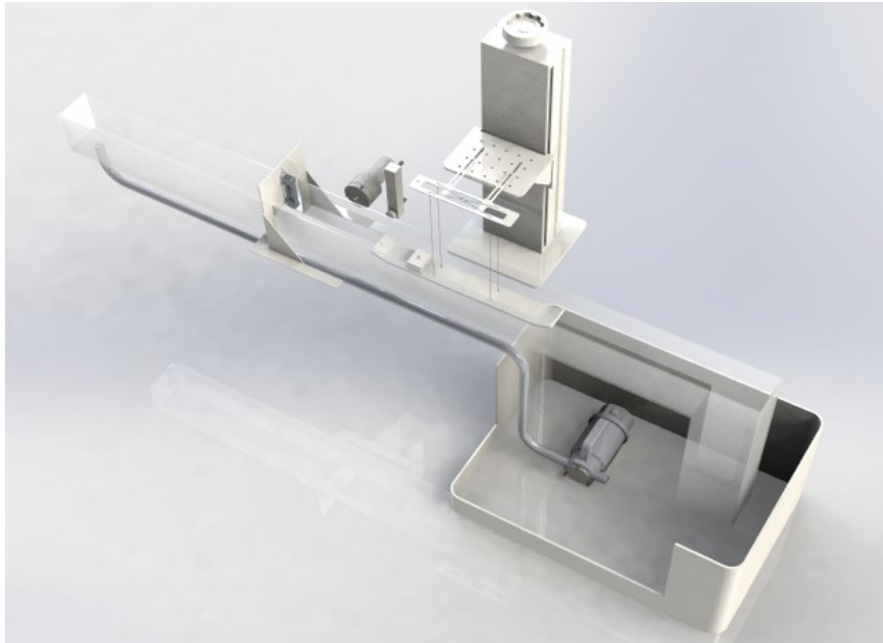


**Figure S1.** Schematic of the underwater drag reduction test system. The system mainly consisted of a water circulation system, a gas supply system, and a force measurement system. The water circulation system consisted of a water tank, a water pump, and an open channel, forming an open channel turbulence loop. The water velocity in the channel was adjusted by the speed control of the water pump and the size control of the outlet. The water velocity was monitored by a flow meter, and the force measurement system used a traction drag plate method to measure the drag reduction rate, the bottom groove of the drag plate could be embedded into the test surface. The front end of the drag plate was connected to a force sensor through a traction rope to directly measure the water flow resistance. The drag plate adapted to changes in liquid level height by connecting to a lifting platform. The gas supply system used a variable frequency air pump to directly supply air, and the air outlet was located at the front end of the upstream position of the drag plate. The airflow meter detected the airflow status. The bottom groove of the drag plate can fix different experiment samples. One side of the drag plate was connected to a force sensor (DYX-306, China Bengbu Sensing System Engineering Co., Ltd.). Underwater freedom gas bubbles were generated by the air pump (ES-3910, China Anyuan Huaqun Technology Co., Ltd.) on the same side of the drag plate connection force sensor.

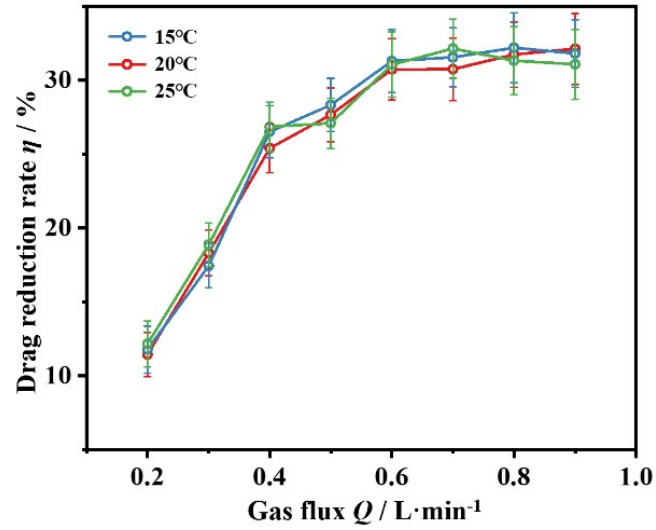


**Fig. S2.** Drag reduction rate of the SPSB at different water temperatures.

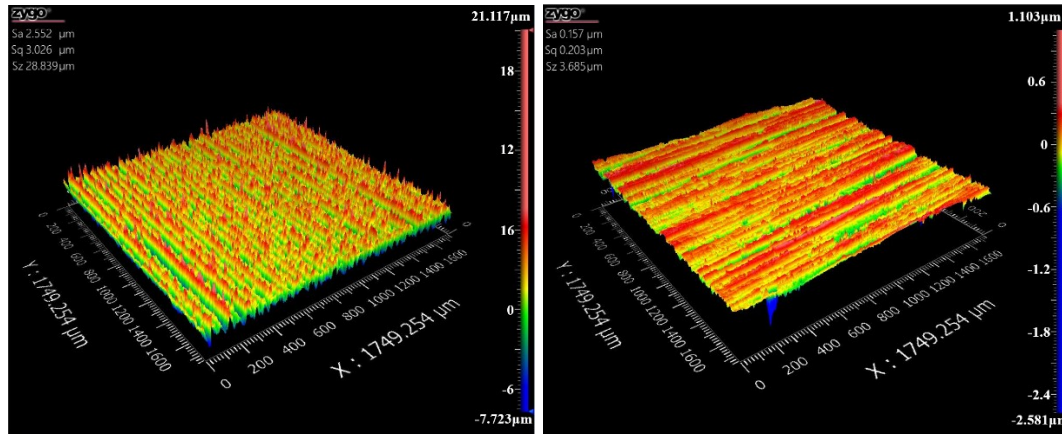


**Fig. S3.** Surface roughness of the exterior area of the track for two types of surfaces. We fabricated an underwater superaerophilic pattern composed of superhydrophobic track and outer superhydrophilic region. The first figure of Figure S3 was the surface profile of superhydrophilic region. The second figure of Figure S3 was the surface profile of hydrophilic region of SPSB.

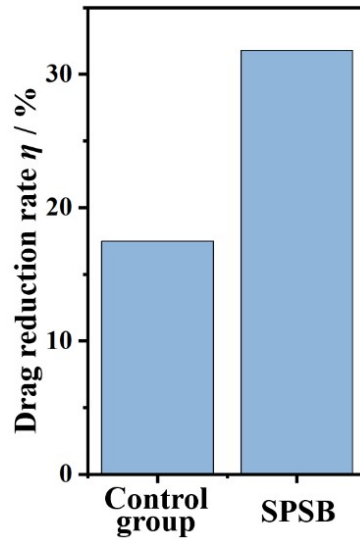


**Fig. S4.** Comparison of drag reduction rates between two different surfaces, where the control group was the underwater superaerophilic pattern composed of superhydrophobic track and outer superhydrophilic region.

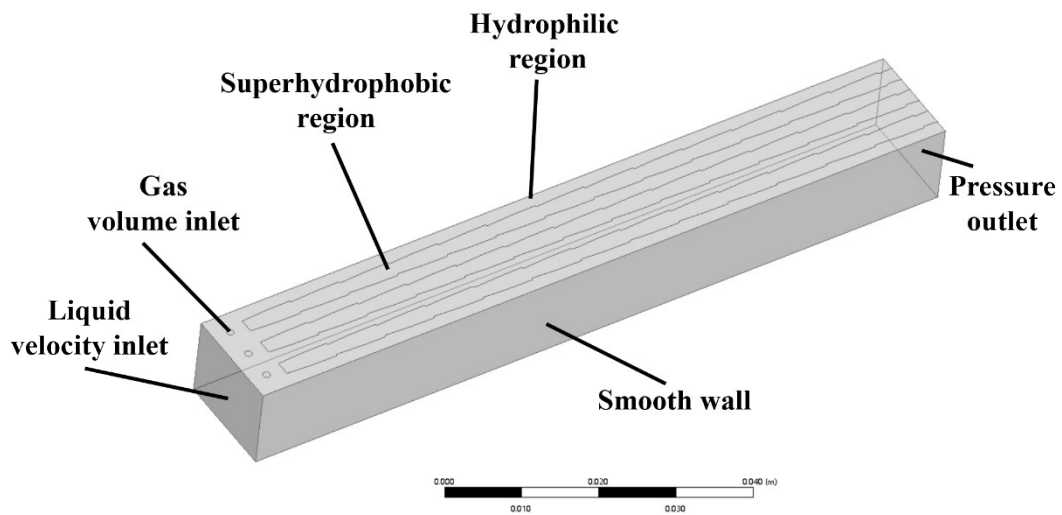


**Figure S5.** Boundary attribute setting of the SPSB numerical simulation model.

Number of Grids: 975951  
Number of nodes: 183457

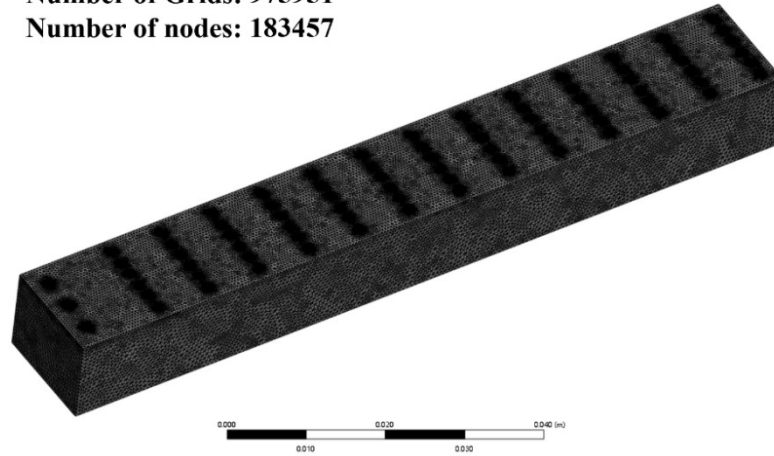


Figure S6. Grid division of the SPSB numerical simulation model.

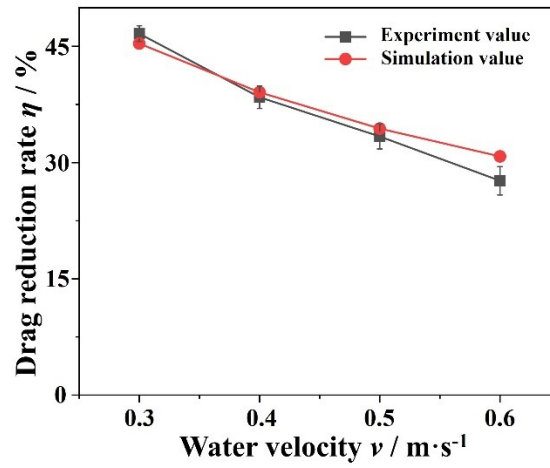


Figure S7. Comparison of the experiment value and simulation value of the SPSB at a gas flux of  $0.5 \text{ L}\cdot\text{min}^{-1}$  and the different water velocities.

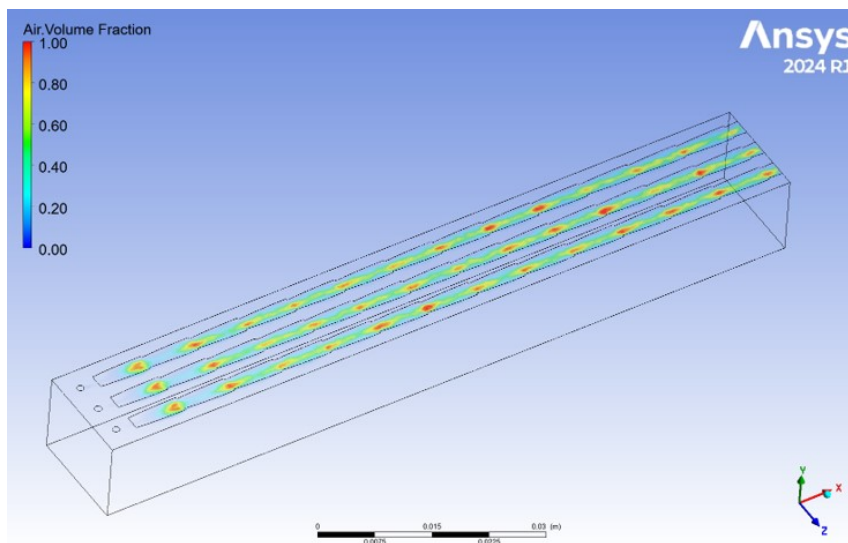
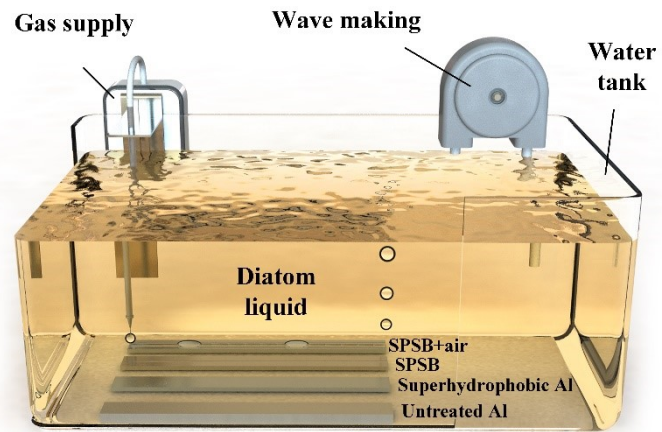
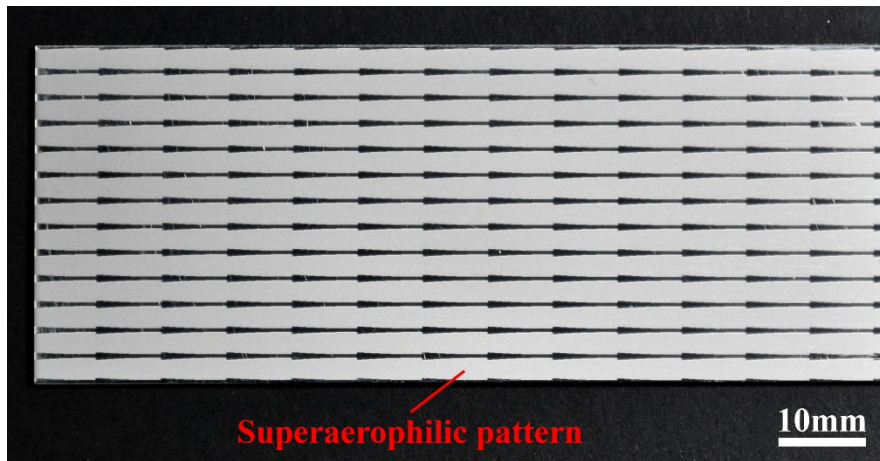


Figure S8. Gas volume fraction cloud map of the SPSB.



**Figure S9.** Schematic of the anti-diatom attachment experimental device.



**Figure S10.** Image of the pattern arrangement when the SPSB can achieve maximum anti fouling area.

## 2. Table section

**Table S1.** Average drag reduction rate of the SPSB at different gas fluxes and  $0.3 \text{ m}\cdot\text{s}^{-1}$  water velocity.

Gas flux / $\text{L}\cdot\text{min}^{-1}$	0.2	0.3	0.4	0.5	0.6	0.7	0.8	0.9
Average drag reduction rate / %	24.59	35.42	40.97	46.65	47.81	49.22	49.88	51.58

**Table S2.** Average drag reduction rate of the SPSB at different gas fluxes and  $0.4 \text{ m}\cdot\text{s}^{-1}$  water velocity.

Gas flux/ $\text{L}\cdot\text{min}^{-1}$	0.2	0.3	0.4	0.5	0.6	0.7	0.8	0.9
Average drag reduction rate / %	18.4	24.29	31.95	38.44	41.51	42.6	43.34	43.21

**Table S3.** Average drag reduction rate of the SPSB at different gas fluxes and  $0.5 \text{ m}\cdot\text{s}^{-1}$  water velocity.

Gas flux/ $\text{L}\cdot\text{min}^{-1}$	0.2	0.3	0.4	0.5	0.6	0.7	0.8	0.9
Average drag reduction rate / %	15.72	21.79	27.79	33.38	36.02	36.62	36.37	37.12

**Table S4.** Average drag reduction rate of the SPSB at different gas fluxes and  $0.6 \text{ m}\cdot\text{s}^{-1}$  water velocity.

Gas flux/ $\text{L}\cdot\text{min}^{-1}$	0.2	0.3	0.4	0.5	0.6	0.7	0.8	0.9
Average drag reduction rate / %	11.43	18.3	25.4	27.66	30.74	30.75	31.75	32.14

**Table S5.** Average drag reduction rate of the hydrophobic Al surface at different gas fluxes and  $0.6 \text{ m}\cdot\text{s}^{-1}$  water velocity.

Gas flux/ $\text{L}\cdot\text{min}^{-1}$	0.2	0.3	0.4	0.5	0.6	0.7	0.8	0.9
Average drag reduction rate / %	3.17	3.63	4.05	6.19	7.83	8.18	9.26	9.75

**Table S6.** Average drag reduction rate of the untreated Al at different gas fluxes and  $0.6 \text{ m}\cdot\text{s}^{-1}$  water velocity.

Gas flux/ $\text{L}\cdot\text{min}^{-1}$	0.2	0.3	0.4	0.5	0.6	0.7	0.8	0.9
Average drag reduction rate / %	3.73	2.92	3.96	5.93	7.37	6.3	8.73	8.31

**Table S7.** Comparison of the drag reduction rate of different methods that reported in the literatures.

Methods	References	Water velocity / $\text{m}\cdot\text{s}^{-1}$	Drag reduction rate / %
Gas lubrication	[1]	0.26	27
	[2]	0.2	20
Bionic skin	[3]	1.5	17.25
	[4]	2	10
	[5]	0.5	10.26
	[6]	0.1	28.5
	[7]	0.6	20
	[8]	2	9.9
Groove	[9]	0.2	30
	[10]	0.3	15
Coating	[11]	6	12.65
	[12]	0.8	25.27

### **3. Video section**

**Video S1.** The transportation processes of the air bubble on the SPSB.

**Video S2.** The gas layer states of the SPSB at different gas fluxes.

**Video S3.** The gas layer states of different surfaces.

**Video S4.** The gas layer states of different inclined surfaces.

**Video S5.** The experimental process of simulating barnacle larvae adhering to the untreated Al surface and SPSB.

## Reference

- 1 G. Liu, Z. Yuan, Z. Qiu, S. Feng, Y. Xie, D. Leng, and X. Tian, *Ocean Eng.*, 2020, **199**, 106962.
- 2 M. D. Ibrahim, S. N. A. Amran, Y. S. Yunus, M. R. A. Rahman, M. Z. Mohtar, L. K. Wong, and A. Zulkharnain, *Appl. Bionics Biomech.*, 2018, 1-11.
- 3 X. Pu, G. Li and Y. Liu, *Chembioeng Rev.*, 2016, **3** (1), 26-40.
- 4 L. Wu, H. Wang, Y. Song, B. Zhang, Y. Xu, C. Liu, and Y. Yan, *Sci. Rep.*, 2020 **10** (1), 12873.
- 5 H. Wang, K. Wang and G. Liu, *Ocean Eng.*, 2022, **258**, 111833.
- 6 D. Saranadhi, D. Chen, J. A. Kleingartner, S. Srinivasan, R. E. Cohen, and G. H. McKinley, *Sci. Adv.*, 2016, **2** (10), e1600686.
- 7 J. Jang, S. H. Choi, S. Ahn, B. Kim, and J. S. Seo, *Int. J. Nav. Archit. Ocean Eng.*, 2014 **6** (2), 363-379.
- 8 T. Min and J. Kim, *Phys. Fluids*, 2004, **16** (7), L55-L58.
- 9 H. Zhang, L. Yin, L. Li, S. Shi, Y. Wang, and X. Liu, *Rsc Adv.*, 2016, **6** (17), 1434-1441 .
- 10 Y. Wang, X. Wang, X. Ma, Z. Tang, and N. Jiang, *Acta Mech. Sin.*, 2022, **38** (10), 322022.
- 11 Y. Liu, H. Zhang, P. Wang, Z. He, and G. Dong, *Mater. Des.*, 2022, **219**, 110765.
- 12 M. Xu, A. Grabowski, N. Yu, G. Kerezyte, J. Lee, B. R. Pfeifer, and C. C. Kim, *Phys. Rev. Appl.*, 2020, **13** (3), 034056.
- 13 B. Wang, J. Wang and D. Chen, *Science China Technological Sciences*, 2013, **56** (12), 2973-2978.
- 14 P. Du, D. Song, F. Ren, Q. Xue, and H. Hu, *J. Appl. Fluid Mech.*, 2017, **10** (2), 491-498.